Multiview three-dimensional display with continuous motion parallax through planar aligned *OLED* microdisplays

Dongdong Teng, Yi Xiong, Lilin Liu,* and Biao Wang

State Key Laboratory of Optoelectronic Materials and Technologies, School of Physics and Engineering, Sun Yat-sen University, Guangzhou 510275, China

**liullin@mail.sysu.edu.cn*

Abstract: Existing multiview three-dimensional (*3D*) display technologies encounter discontinuous motion parallax problem, due to a limited number of stereo-images which are presented to corresponding sub-viewing zones (*SVZ*s). This paper proposes a novel multiview *3D* display system to obtain continuous motion parallax by using a group of planar aligned *OLED* microdisplays. Through blocking partial light-rays by baffles inserted between adjacent *OLED* microdisplays, transitional stereo-image assembled by two spatially complementary segments from adjacent stereo-images is presented to a complementary fusing zone (*CFZ*) which locates between two adjacent *SVZ*s. For a moving observation point, the spatial ratio of the two complementary segments evolves gradually, resulting in continuously changing transitional stereo-images and thus overcoming the problem of discontinuous motion parallax. The proposed display system employs projection-type architecture, taking the merit of full display resolution, but at the same time having a thin optical structure, offering great potentials for portable or mobile *3D* display applications. Experimentally, a prototype display system is demonstrated by 9 *OLED* microdisplays.

OCIS codes: (330.1400) Vision - binocular and stereopsis; (120.2040) Displays.

References and links

1. J. Y. Son and B. Javidi, "Three-dimensional imaging methods based on multi-view images," J. Disp. Technol. **1**(1), 125–140 (2005).
2. J. Y. Son, V. V. Saveljev, J. S. Kim, S. S. Kim, and B. Javidi, "Viewing zones in three-dimensional imaging systems based on lenticular, parallax-barrier, and microlens-array plates," Appl. Opt. **43**(26), 4985–4992 (2004).
3. D. Lanman, M. Hirsch, Y. Kim, and R. Raskar, "Content-adaptive parallax barriers: optimizing dual-layer 3D displays using low-rank light field factorization," ACM Trans. Graph. **29**(6), 163–172 (2010).
4. Y. Takaki, O. Yokoyama, and G. Hamagishi, "Flat panel display with slanted pixel arrangement for 16-view display," In Stereoscopic Displays and Applications XX, A. Woods, N. Holiman, and J. Merrittl, eds, Proc. SPIE-IS& T Electronic Imaging **7237**, 723708 (2009).
5. L. Bogaert, Y. Meuret, S. Roelandt, A. Avci, H. De Smet, and H. Thienpont, "Demonstration of a multiview projection display using decentered microlens arrays," Opt. Express **18**(25), 26092–26106 (2010).
6. C. van Berkel, D. W. Parker, and A. R. Franklin, "Multiview 3D LCD," Proc. SPIE **2653**, 32–39 (1996).
7. K. H. Yoon, H. K. Ju, I. K. Park, and S. K. Kim, "Determination of the optimum viewing distance for a multi-view auto-stereoscopic 3D display," Opt. Express **22**(19), 22616–22631 (2014).
8. S. Iwasawa, M. Kawakita, S. Yano, and H. Ando, "Implementation of autostereoscopic HD projection display with dense horizontal parallax," Proc. SPIE **7863**, 78630T (2011).
9. N. A. Dodgson, J. R. Moore, S. R. Lang, G. Martin, and P. Canepa, "A time-sequential multi-projector autostereoscopic 3D display," J. Soc. Inf. Disp. **8**(2), 169–176 (2000).
10. J. Reitterer, F. Fidler, G. Schmid, T. Riel, C. Hambeck, F. Saint Julien-Wallsee, W. Leeb, and U. Schmid, "Design and evaluation of a large-scale autostereoscopic multi-view laser display for outdoor applications," Opt. Express **22**(22), 27063–27068 (2014).
11. S. P. Hines, "Autostereoscopic video display with motion parallax," Proc. SPIE **3012**, 208–219 (1997).
12. J. Geng, "Three-dimensional display technologies," Adv. Opt. Photon. **5**(4), 456–535 (2013).
13. C. van Berkel and J. A. Clarke, "Characterization and optimization of 3D-LCD module design," Proc. SPIE

#232272 - $15.00 USD Received 12 Jan 2015; revised 15 Feb 2015; accepted 19 Feb 2015; published 25 Feb 2015

3012, 179–186 (1997).
14. Y. Takaki and N. Nago, "Multi-projection of lenticular displays to construct a 256-view super multi-view display," Opt. Express **18**(9), 8824–8835 (2010).
15. Y. Kajiki, H. Yoshikawa, and T. Honda, "Hologram-like video images by 45-view stereoscopic display," Proc. SPIE **3012**, 154–166 (1997).
16. S. H. Ju, M. D. Kim, M. S. Mark, K. T. Kim, J. H. Park, and K. M. Lim, "Viewer's eye position estimation using single camera," SID Syposium Dig. Tech. Pap. **44**(1), 671–674 (2012).
17. P. Surman, R. S. Brar, I. Sexton, and K. Hopf, "MUTED and HELIUM3D autostereoscopic displays," IEEE Intervational Conference on Multimedia and Expo (ICME) 1594–1599 (2010).
18. O. Eldes, K. Akşit, and H. Urey, "Multi-view autostereoscopic projection display using rotating screen," Opt. Express **21**(23), 29043–29054 (2013).
19. Y. Takaki and H. Nakanuma, "Improvement of multiple imaging system used for natural 3D display which generates high-density directional images," Proc. SPIE **5243**, 42–49 (2003).

1. Introduction

Through simultaneously presenting multiple perspective views (stereo-images) of a three-dimensional (*3D*) object, the glasses-free multiview *3D* display creates multiple sub-viewing zones (*SVZ*s), i.e. a spatial region around the viewpoint of each stereo-image. A pupil arriving at each *SVZ* can perceive the corresponding stereo-image, which makes the viewer perceive different stereo-image pairs as his/her left and right eyes moving into corresponding *SVZ*s. Thus, the multiview *3D* display evokes both stereo parallax and motion parallax depth cues of the viewers. This technology is compatible with existing flat two-dimensional (*2D*) display panels. So, the glasses-free multiview *3D* display technology is developing very rapidly in recent years and begins to occupy a prominent position in *3D* display area. According to mechanisms adopted for delivering each stereo-image to corresponding *SVZ*, the multiview *3D* display techniques can be generally categorized as contact-type and projection-type [1, 2]. The contact-type system bases on thin optical plates, such as lenticular [3–5] and parallax barrier [6, 7] plates, to form *SVZ*s, which makes it be suitable for portable or mobile *3D* display products. But pixels of the flat display panel are shared by all the stereo-images, resulting in a rapid decrease of the display resolution when more *SVZ*s are pursued. The projection-type system usually employs multiple projectors [8] or uses one fast switching projector being mated with a screen which provides optical functions for sequential stereo-images [9, 10]. Although it can provide a full display resolution, i.e. being equal to the adopted projector, it is difficult to be packaged into a small-size structure due to the necessary optical adjustment structure.

Inherently, both contact-type and projection-type multiview *3D* display systems only provide a limited number of *SVZ*s. So, the stereo-image viewed by a pupil does not change until the pupil moves to the adjacent *SVZ*. The motion parallax thus appears in a stepwise fashion, degrading the effectiveness of *3D* displays. Overlapping adjacent *SVZ*s by some extent may be able to alleviate this discontinuity as mentioned in ref [11], but such overlap will increase the blurriness of the displayed images [12], especially when the overlapping percent reaches 100% [13]. Furthermore, the presented light intensities in the overlapped zone are difficult to control accurately, resulting in an obvious light intensity fluctuation. The obtained continuity of motion parallax is thus at a coarse level. At present, super-multiview display technique and viewer-tracking technique have been proposed to bypass the discontinuous motion parallax issue. The super-multiview display, featured by a great number of *SVZ*s with an interval smaller than the pupil diameter [14, 15], demands super high resolution or ultra large quantity of *2D* display panels. Viewer-tracking technique [16–18] only accommodates limited viewers and also encounters difficulties for outdoor application due to complex environments.

In this paper, we propose a novel multiview *3D* display system to realize continuous motion parallax by using only a moderate number of planar aligned *OLED* microdisplays without a viewer-tracking unit. Through appropriately offsetting multiple planar aligned lenses, stereo-images from different microdisplays overlap in a virtual displaying plane and

#232272 - $15.00 USD Received 12 Jan 2015; revised 15 Feb 2015; accepted 19 Feb 2015; published 25 Feb 2015

share a common spatial-spectrum plane which serves as the observation plane P_{observ}. Through blocking partial microdisplay light-rays by the baffles, a complementary fusing zone (*CFZ*) gets generated between adjacent *SVZ*s. When a pupil moves across the *CFZ*, continuously changing transitional stereo-images tiled by two segments from adjacent stereo-images are presented, and thus help to make the observed content evolving spatially from one stereo-image to its adjacent stereo-image gradually. So, discontinuous motion parallax gets overcome. Taking full advantages of the inherent large divergence angle of *OLED* pixels, very small light intensity fluctuation on the observing plane guarantees successful continuous motion parallax. The proposed system not only can present stereo-images with full display resolution, but also has a thin optical structure, thus offering great potentials for portable or mobile *3D* display product applications.

The rest of this paper is organized as follows. In section 2, the theory of the proposed novel multiview *3D* display technology for continuous motion parallax is explained. The experimental set up and results are shown in Section 3. Section 4 analyzes the spatial viewing zone along the *z*-direction that is provided by the proposed display system to the viewer. Section 5 provides conclusions.

2. Theory of the multiview *3D* display system with continuous motion parallax

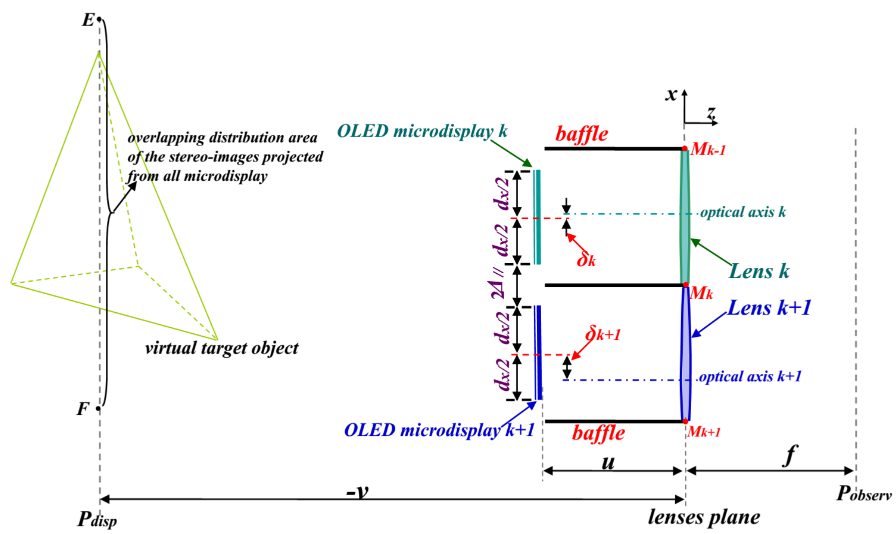

Fig. 1. Optical structure of the proposed multiview display system. Two *OLED* microdisplays are drawn here to demonstrate the proposed ideas.

Figure 1 shows the optical structure of the proposed multiview *3D* display system in the horizontal *x*-*z* plane. An array of planar aligned *OLED* microdisplays with a display area $d_x \times d_y$ are imaged by an array of planar aligned lenses (f). For simplicity, only two *OLED* microdisplays (*OLED* microdisplay k and $k + 1$) and two corresponding lenses (Lens k and $k + 1$) are drawn in the figure. The horizontal interval between adjacent microdisplays is denoted as $d_x + 2\Delta_{\|}$. Through designing the specific offset value of each lens's optical axis with respect to the corresponding microdisplay (δ_k for *OLED* microdisplay k), magnified virtual images of the messages loaded on different *OLED* microdisplays coincide on the P_{disp} as stereo-images. The magnification is determined by $\beta = v/u$, where u represents the object distance and $-v$ denotes the image distance. Points E and F are the common marginal points of the stereo-images along the horizontal *x*-direction, or in other word, the *EF* zone represents the overlapping distribution area of the stereo-images projected from each microdisplay. The lenses are processed into rectangular shape with a horizontal size of $d_x + 2\Delta_{\|}$ for seamless alignment along the *x*-direction. All the lenses and microdisplays are perpendicular with the *z*-

#232272 - $15.00 USD Received 12 Jan 2015; revised 15 Feb 2015; accepted 19 Feb 2015; published 25 Feb 2015

direction. M_{k-1}, M_k and M_{k+1} are the joined points of adjacent lenses. The common spatial-spectrum plane, i.e. the common focal plane of all the lenses, serves as the observation plane P_{observ}. A group of baffles are inserted between adjacent microdisplay-lens combination units to block the *OLED* microdisplay light-rays which exceed the corresponding lenses. Along the *z*-axis, they are confined in between the lenses and the microdisplays.

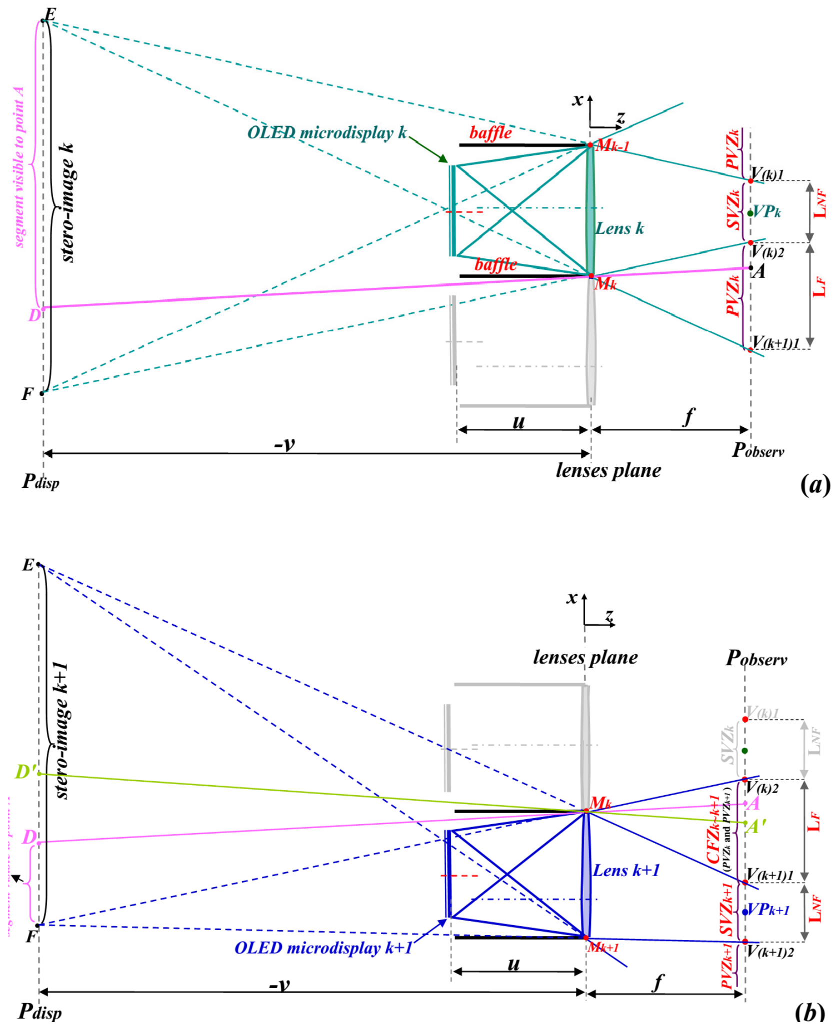

Fig. 2. Optical structures of the proposed multiview *3D* display system with only two microdisplay-lens combination units for simplicity: (a) Only *OLED* microdisplay *k* being activated by stereo-image *k*; (b) Only *OLED* microdisplay *k* + 1 being activated by stereo-image *k* + 1.

When only *OLED* microdisplay *k* is activated, the virtual stereo-image *k* is projected to the *EF* zone, as shown in Fig. 2(a). Due to usage of the baffles, partial light-rays of the microdisplay *k* which exceed the Lens *k* are blocked. It implies that the aperture of the Lens *k* plays the role of an optical pupil to the stereo-image *k*. The light-rays from the stereo-image *k* pass through the optical pupil freely, but get blocked once they exceed the optical pupil. According to geometric optics, the passing-through light-rays form two kinds of zones on the P_{observ}: $V_{(k)1}V_{(k)2}$ zone and $V_{(k)2}V_{(k+1)1}$ zone. Here $V_{(k)1}$, $V_{(k)2}$, and $V_{(k+1)1}$ are the intersection points of line EM_{k-1}, FM_{k-1}, and EM_k with the P_{observ}. For each observation points in the

#232272 - $15.00 USD Received 12 Jan 2015; revised 15 Feb 2015; accepted 19 Feb 2015; published 25 Feb 2015

$V_{(k)1}V_{(k)2}$ zone, the whole stereo-image k is visible. This zone is denoted as sub-viewing zones k (SVZ_k). But for an observation point in the $V_{(k)2}V_{(k+1)1}$, e.g. point A, only a segment of the stereo-image k, *i.e.* ED segment of the stereo-image k, is visible. That is to say, for any point in this zone, only a partial stereo-image k is visible. So, the $V_{(k)2}V_{(k+1)1}$ zone is denoted as partial-stereo-image viewing zone k (PVZ_k) here. Actually, there exist two PVZ_k zones adhering to the SVZ_k zone from two sides.

Similarly, when only *OLED* microdisplay $k + 1$ gets activated by the stereo-image $k + 1$, a SVZ_{k+1} zone where the whole stereo-image $k + 1$ is visible and two PVZ_{k+1} zones where only a partial stereo-image $k + 1$ is visible get generated on the P_{observ}, as shown in Fig. 2(b). Due to the seamless planar alignment of the Lenses k and $k + 1$, between SVZ_k and SVZ_{k+1}, a PVZ_k zone and a PVZ_{k+1} zone overlap with each other completely. This overlapping zone is defined as the complementary fusing zone $k\sim k+1$ ($CFZ_{k\sim k+1}$) in this paper. For an observation point A in the $CFZ_{k\sim k+1}$, the DF segment of stereo-image $k + 1$ gets visible.

Based on above discussions, when the microdisplays k and $k + 1$ are activated simultaneously by the stereo-images k and $k + 1$, respectively, the ED segment of stereo-image k and the DF segment of stereo-image $k + 1$ are presented to point A simultaneously, as shown in the left part of the Fig. 3. The two segments link up at the point D seamlessly, spatially tiling up a transitional stereo-image. The nomination of the CFZ is based on the spatially complementary characteristics of the two segments. Under this condition, two SVZs and one CFZ constitute a horizontal viewing zone in a spatial end to end manner. The center points of each SVZ, i.e. VP_k and VP_{k+1} in Fig. 2, are taken as the viewpoints of the corresponding stereo-images. For example, the stereo-image k is the projection view of the target object converging to VP_k. As shown in Fig. 1, the target object is virtually located between point E and F around the P_{disp}. The horizontal sizes of the SVZ and CFZ zones are calculated geometrically as:

$$\begin{aligned} L_{NF} &= 2(f/u)\Delta_{\parallel} \\ L_F &= (f/u)d_x \end{aligned} \tag{1}$$

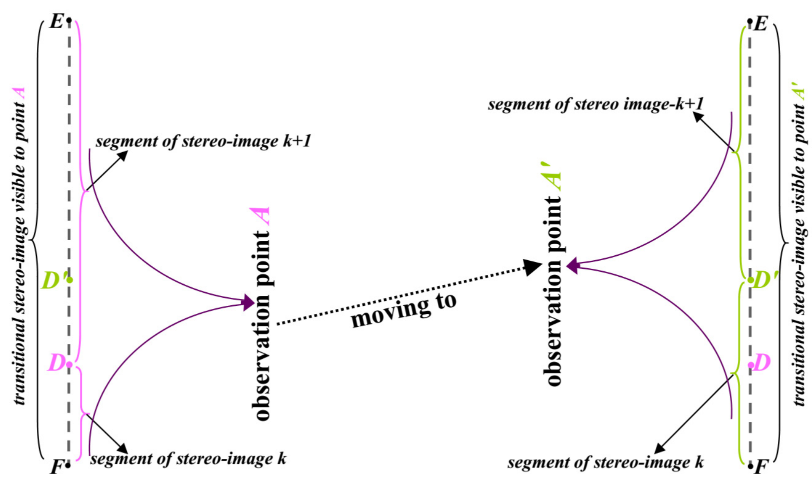

Fig. 3. The spatially changing transitional stereo-images observed by a moving observation point at different positions of a CFZ. The observation points A and A' are as denoted in the Fig. 2(b).

For a point in the SVZ zone, light-rays passing through the point are from all displayed pixels of the corresponding stereo-image. For a point in the CFZ zone, light-rays passing through the point are from all displayed pixels of the corresponding transitional stereo-image. Because the transitional stereo-image is tiled by two complementary segments from two

#232272 - $15.00 USD Received 12 Jan 2015; revised 15 Feb 2015; accepted 19 Feb 2015; published 25 Feb 2015

adjacent stereo-images, it has a resolution equal to the stereo-image and the number of light-rays passing through these two kinds of points is identical. The light emission from each *OLED* pixel inherently has a very large divergence angle. After transmitting through the lens with a limited aperture, each light ray presents an approximately homogeneous light intensity distribution on the P_{observ}. Thus, for any point in the horizontal viewing zone, a uniform light intensity distribution gets guaranteed.

The joint point D of the transitional stereo-image is in fact the intersection point of the line AM_k with the P_{disp}, which does linkage movement with the observation point but toward the reverse direction. For example, when the observation point A moves toward A' along the negative direction of x-axis, the joint point D shifts toward D' along the positive direction, as shown in Fig. 2(b). As to the observed transitional stereo-image, the segment from the stereo-image k shrinks to ED' zone and the segment from the stereo-image $k + 1$ expands to $D'F$ zone, as shown in Fig. 3. That is to say, for an observation point moving along the *CFZ* zone, the spatial ratio of the observed two complementary segments from different stereo-images changes from 1:0 to 0:1 gradually. Consequently, a continuously changing transitional stereo-image gets realized for a moving observation point. With the help of the continuously changing transitional stereo-image, the observed image will evolve from a complete stereo-image k to a complete stereo-image $k + 1$ in a spatial "point by point" manner when the observation point moves from SVZ_k to SVZ_{k+1}. As discussed above, the light intensity distribution in the horizontal viewing zone is approximately homogeneous. So the observed image shows no obvious light intensity fluctuation for a moving observation point.

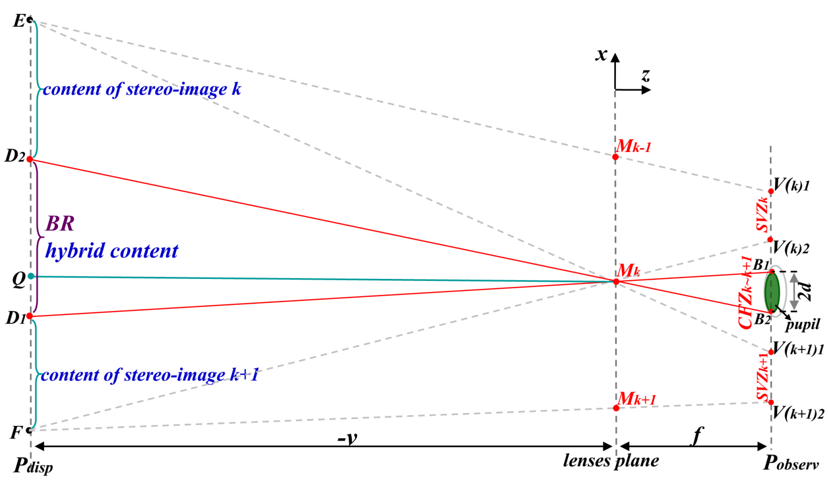

Fig. 4. Optical diagram showing the observed transition stereo-image when the pupil is covered by a *CFZ*.

Actually, the pupil of a viewer is an aperture, not a point as discussed above. Replacing the observation point by a pupil of diameter $2d$, the joint point D will grow into a region, denoted as a blending region (*BR*) in this paper. As shown in Fig. 4, for a pupil in the $CFZ_{k\sim k+1}$ with marginal points B_1 and B_2 along the horizontal direction, the marginal points (D_1 and D_2) of the *BR* will be on the extension lines of B_1M_k and B_2M_k. Outside the *BR*, each point in the ED_2 or D_1F presents the image content of the stereo-image k or $k + 1$ to the pupil, respectively. However, within the *BR*, the presented content of each point is a hybrid of the two stereo-images' contents by a spatially varied percent. Specifically, the presented content of a point Q in the *BR* is

$$I_Q = \alpha_{Qk} I_Q^k + \alpha_{Qk+1} I_Q^{k+1} \tag{2}$$

where I_Q^k and I_Q^{k+1} represent the contents included in the point Q coming from the stereo-image k and $k + 1$, respectively. The weight factors α_{Qk} and α_{Qk+1} depend on the position of the point Q, evolving spatially and continuously:

$$\begin{aligned} \alpha_{Qk} &= D_2Q / D_2D_1 \\ \alpha_{Qk+1} &= QD_1 / D_2D_1 \\ D_2D_1 &= 2(\beta - 1)d \end{aligned} \tag{3}$$

So, from point D_2 to D_1, the image content presented to the pupil changes spatial-gradually from the content of the stereo-image k to that of the stereo-image $k + 1$. Obviously, for a pupil, the number of segments building up the transitional stereo-image increases from two to three compared with the situation of an observation point.

In fact, when a pupil moves from the viewpoint k to its adjacent viewpoint $k + 1$, there are three kinds of situations. In situation *I*, the pupil is completely covered by the SVZ_k and the whole stereo-image k is observed. In situation *II*, the pupil straddles SVZ_k and $CFZ_{k\sim k+1}$, as shown in Fig. 5. The intersection point of the line B_2M_k with P_{disp} is denoted as D_3. Here, B_2 is the marginal point of the pupil in the $CFZ_{k\sim K+1}$. The transitional stereo-image is built up by two segments. A segment, denoted as ED_3, presents contents of the stereo-image k. The complementary segment, D_3F, works as the *BR*. For a point Q' in the *BR*, the presented content is expressed as:

$$I_{Q'} = \alpha_{Q'k} I_{Q'}^k + \alpha_{Q'k+1} I_{Q'}^{k+1} \tag{4}$$

where the weight factors are calculated by

$$\begin{aligned} \alpha_{Qk+1} &= Q'D_3 / (2(\beta - 1)d) \\ \alpha_{Qk} &= 1 - \alpha_{Qk+1} \end{aligned} \tag{5}$$

The situation *III* is as given by Fig. 4. Above processes can be generalized for pupil's movement from one viewpoint to its adjacent viewpoint along the + x or –x direction.

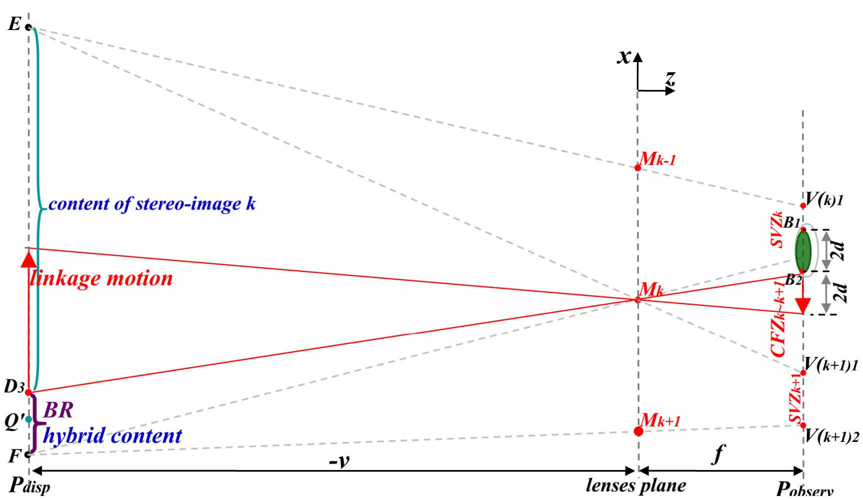

Fig. 5. Optical diagram showing the observed transition stereo-image when the pupil straddles the adjacent *SVZ* and *CFZ*.

Equations (2)–(5) mathematically indicate that the content of each display point presented to a moving pupil experiences a timed gradual process as the *BR* sweeps across. In other

#232272 - $15.00 USD Received 12 Jan 2015; revised 15 Feb 2015; accepted 19 Feb 2015; published 25 Feb 2015

words, for example, the point D_3 in Fig. 5 is at the upper edge of the *BR*, it presents the content of stereo-image *k*. When the pupil translates a distance of *2d* (the diameter of the pupil) along the negative direction of *x*-axis, the point D_3 becomes the lower edge of the *BR*, i.e. "D_1" in Fig. 4 of the situation *III*. The presented content changes to that of the stereo-image $k + 1$. With the pupil's movement, the content presented by the point D_3 changes from the content of the stereo-image *k* to that of the stereo-image $k + 1$ timed gradually.

In summary, all above analysis clearly shows that the observed changes continuously from the stereo-image *k* to the stereo-image $k + 1$ when the pupil moves from a viewpoint *k* to the adjacent viewpoint $k + 1$. This evolution process takes place not only by a spatial "point by point" way for the whole observed image, but also by a timed gradual way for the presented content of each display point of the observed image.

Introducing more *OLED* microdisplays into the proposed system, more *SVZ*s and *CFZ*s will be formed. En route continuously changing transitional stereo-images, a multiview *3D* display with continuous motion parallax will be implemented if only all linked *SVZ*s and *CFZ*s can cover two pupils of a viewer. In the case of $2m + 1$ microdisplays with $(2m + 1) + 1$ baffles being inserted, numbered as $-m$, $-(m-1)$, $\cdots$, 0, $\cdots (m-1)$, m, there will be $2m + 1$ *SVZ*s and $2m$ *CFZ*s constructing the horizontal viewing zone (*VZ*) of the system. Symmetrically, lets the offset $\delta_0 = 0$. As shown in the Fig. 6, the mid-point of the microdisplay *0*, C_0, and the mid-point of the line-segment *EF*, *C*, are on the optical axis of the lens *0*. To guarantee the overlapping of images of all *OLED* microdisplays, the mid-point of the marginal microdisplay *m*, C_m, should be imaged to the point *C* by the corresponding Lens *m*. According to the geometry relationship, the line CC_m passes through the optical center of the Lens *m*. The maximum offset of the microdisplay *m* with respect to the corresponding lenses can be expressed geometrically as:

$$\beta\delta_m = \delta_m + m(d_x + 2\Delta_{\parallel}) \Rightarrow \delta_m = m(d_x + 2\Delta_{\parallel}) / (\beta - 1) \tag{6}$$

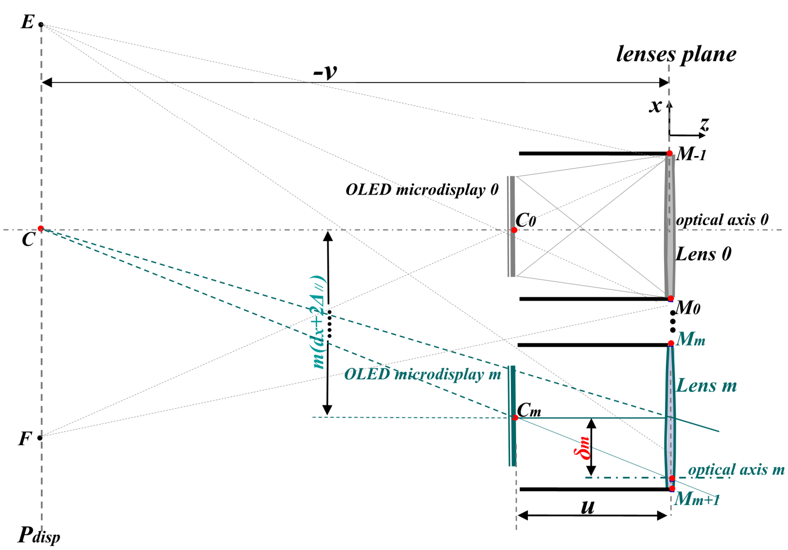

Fig. 6. Optical diagram showing the offsetting of the optical axis of the Lens *m* with respect to the corresponding microdisplay.

Equation (6) is also feasible for calculating the offset value of other lens's optical axis with respect to the corresponding microdisplay when the *m* is replaced by the subscript number of the corresponding microdisplay.

The rectangular lenses are cut down from a group of mother lenses with identical characteristics. To collect light-rays between adjacent baffles, along the horizontal direction, the aperture size of the mother lens should not be less than:

$$A_x = 2(\delta_k + (d_x + 2\Delta_{\parallel})/2) = (2m + \beta - 1)(d_x + 2\Delta_{\parallel})/(\beta - 1) \quad (7)$$

So, the number of microdisplays accommodated in the proposed system is limited by:

$$\left.\begin{array}{l} Eq.(7) \\ N.A. > A_x / f \end{array}\right\} \Rightarrow 2m + 1 < [(f \times N.A.)(\beta - 1)/(d_x + 2\Delta_{\parallel}) - (\beta - 2)] \quad (8)$$

To obtain a thin optical structure, a small f is preferred. The parameters $2\Delta_{\parallel}$ and β have small influences on the number $2m + 1$ mathematically. So, the parameters $N.A.$ and d_x play key roles on the value of $2m + 1$.

As discussed above, $2m + 1$ *SVZ*s and $2m$ *CFZ*s construct a horizontal *VZ* with a size of $(2m + 1)L_{NF} + 2mL_F$. Thus, the viewing angle of the *3D* object displayed by the proposed system, i.e. the field angle of the *VZ* to the *EF* zone, can be calculated approximately by:

$$Viewing\ Angle \approx \arcsin\left[((2m+1)L_{NF} + 2mL_F)/(-v + f)\right] \quad (9)$$

Obviously, more microdisplays would bring a wider horizontal viewing angle. Equations (8) and (9) together lead to the conclusion that the viewing angle of the *3D* object displayed by the proposed system is determined by the *N.A.* of the used lenses when d_x is a constant value.

3. Experiments and results

A display system is set up to implement the idea described above, as shown in Fig. 7. Nine white *OLED* microdisplays, with a display area $d_x \times d_y = 10.08 \times 7.56 mm^2$ and a resolution 800 × 600, from *OLEiD of China* are used. To show the inner structure more clearly, four of the ten baffles are removed for photograph. Since each *OLED* microdisplay device is packaged with a driving board individually, its mechanical size is $22 \times 17 mm^2$. Aligning microdisplays side by side, the value of $2\Delta_{\parallel}$ reaches 11.92*mm*. According to Eq. (1), the width of the sub-viewing zone L_{NF} is much larger than the pupil diameter, which is about 3*mm* at indoor environments. The pupil will receive an invariant stereo-image until it moves out of a *SVZ,* which will deteriorate continuous motion parallax. In order to reduce the width of the *SVZ*, nine *OLED* microdisplays are arranged into two parallel rows alternatively. The vertical interval between the two rows is set as $d_y + 2\Delta_{\perp} = 17.6mm$, a little larger than the vertical mechanical size of the microdisplay, which makes sure adjacent microdisplays (one in the upper row and another in the lower row) have no spatial conflict along the horizontal direction. Thus, the horizontal interval between adjacent microdisplays is reduced to 13*mm* in favor of a smaller width of the *SVZ*.

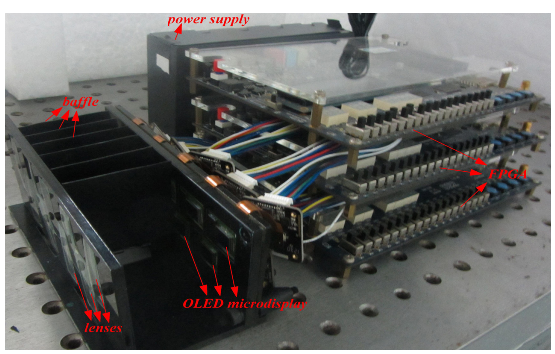

Fig. 7. Photograph of the experimental display system.

#232272 - $15.00 USD Received 12 Jan 2015; revised 15 Feb 2015; accepted 19 Feb 2015; published 25 Feb 2015

To guarantee overlapping of all stereo-images, the optical axises of the two rows of lenses should be arranged by an offset $\delta_y = \pm\,(8.8/(\beta\text{-}1))mm$ with respect to the vertical geometrical center of the corresponding microdisplays. The vertical viewing zones (VZ_u and VZ_l) of microdisplays belonging to different rows exhibit misplacement. Their overlapped region defines the vertical range ($VZ_{\perp}$) of the viewing zone where the whole stereo-image or transitional stereo-image are visible, as shown in Fig. 8.

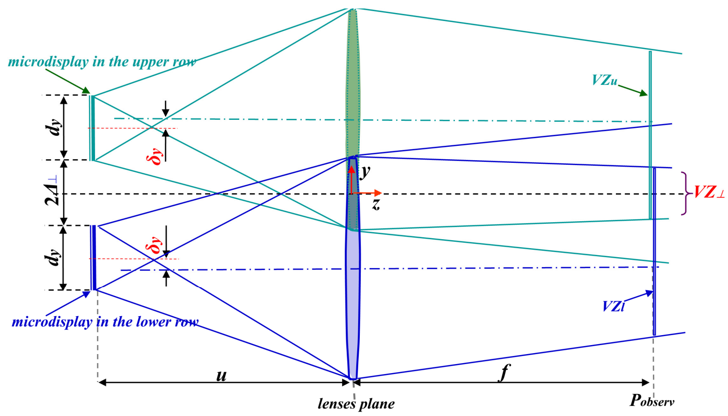

Fig. 8. Schematic diagram showing the vertical viewing zone of the display system.

Choosing achromatic lenses with an effective aperture 45*mm*, i.e. *N.A* = 0.75, as mother lenses, 9 kinds of rectangular parts, with a size of 13 × 36mm^2 to satisfy Eq. (7), are cut out from these mother lenses and processed into the rectangular lenses for usage in our experiment. Their geometrical centers are 0, $\pm(d_x + 2\Delta_{\|})/(\beta-1)$, $\pm 2(d_x + 2\Delta_{\|})/(\beta-1)$, $\pm 3(d_x + 2\Delta_{\|})/(\beta-1)$ and $\pm 4(d_x + 2\Delta_{\|})/(\beta-1)$ away from the geometric center of the mother lenses along the horizontal direction, respectively.

Other system parameters include f = 60*mm*, u = 160/3*mm*. Under this condition, β = 9, v = −480*mm*, L_{NF} = 3.285*mm*, L_F = 11.34*mm*, the vertical range of the *VZ* is 9.72*mm* and the available size of the stereo-image is 90.72 × 68.04mm^2. The thickness of the optical structure is as small as 65*mm*. For symmetric consideration, the displayed *3D* object is set as 68 × 68 × 68mm^3. The horizontal range of the *VZ* is 120.285*mm,* which is about 1.9 times as large as the average interocular distance (64*mm*) of a viewer. According to Eq. (9), a viewing angle of about 13° is reached by the proposed system.

A uniform light intensity distribution on the P_{disp} is a necessary condition for the proposed system. The inherent light emission characteristics of *OLED*, i.e. large divergence angle, guarantees this point. With all the microdisplays being active and all the pixels being set at the maximum intensity value, the light intensity distribution in the viewing zone is measured at a step interval of 3*mm* along the *x*-direction by a luminance meter *CS-2000A* from *Konicaminolta*. Figure 9 shows the measured values and a small light intensity fluctuation (<2%) is confirmed. So, intensities of the observed different stereo-image or transitional stereo-images are nearly uniform. The perceived image for a moving pupil is free from intensity fluctuation.

#232272 - $15.00 USD Received 12 Jan 2015; revised 15 Feb 2015; accepted 19 Feb 2015; published 25 Feb 2015

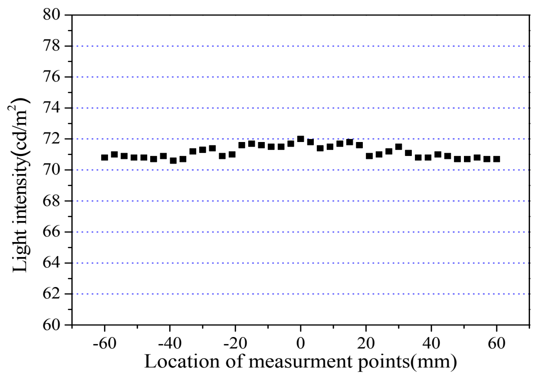

Fig. 9. Measured light intensities along the horizontal center line of the viewing zone.

To exhibit how a transitional stereo-image is tiled spatially, a verification experiment is performed. A research-type *CCD* (SenSys *1602E*) is put in the $CFZ_{0\sim1}$ to capture the presented image. For a transitional stereo-image from *OLED* microdisplay *k* and *k* + *1,* if only one of them being activated at each time, the presented images are fragments of the transitional stereo-image. Figure 10(a) and 10(b) show the captured images when one of microdisplays *0* and *1* is activated by its corresponding stereo-image. Figure 10(c) shows the captured image when both of them are activated. Obviously, Fig. 10(c) is the spatial tilling of the former two. In our experiment, the diaphragm of the *CCD* is always set as 3*mm*, which is the average pupil diameter at indoor environments.

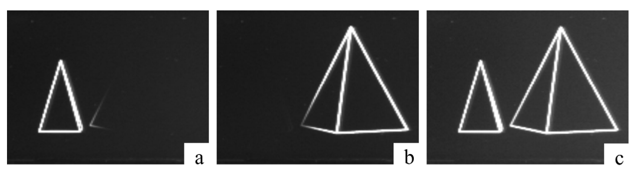

Fig. 10. Captured transitional stereo-images at a observation position in the $CFZ_{0\sim1}$ when (a)only the microdisplay *0* is active, (b) only the microdisplay *1* is active and (c)both of them are active.

Two pyramids are displayed to demonstrate the proposed idea and system. Let the CCD be at ten positions with an equal interval along the horizontal direction in the *VZ*, captured images are shown in Fig. 11. A more intuitive feeling can be obtained through seeing the online multimedia recorded by a camera translating at a constant speed along the horizontal direction (Media 1). When the *B*R sweeps across the *SVZ*s, the change rate of the observed transitional stereo-image becomes slow, as can be seen in the multimedia, which is due to the blank parts (i.e. no message) in the display zone for the stereo-images and the existence of the *SVZ*s. This phenomenon can be alleviated by adopting full filled stereo-images and *SVZ*s with a small size. Whatever, the change is still continuous. Five subjects observed the displayed *3D* image in the lab environment and no obvious discontinuous motion parallax was perceived.

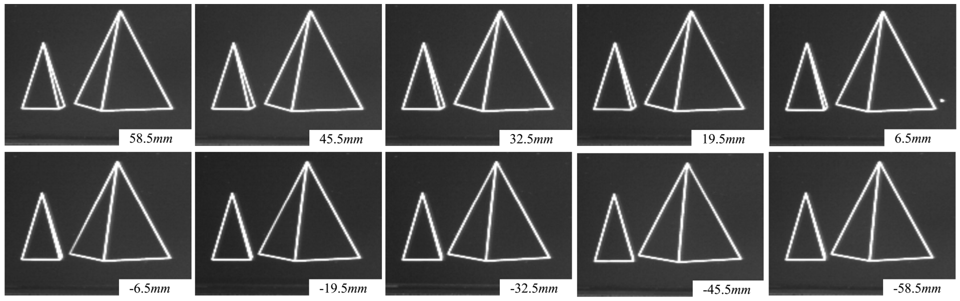

Fig. 11. Captured images with a spatial interval of 13*mm* along the horizontal direction when the proposed display system works. The labels on each image denote the shooting position, with 0*mm* representing the midpoint of the viewing zone. A more intuitive feeling can be found in the online multimedia (Media 1).

4. Discussions on the spatial range of the *VZ* along the *z*-direction

In above paragraphs, the discussed *SVZ*s and *CFZ*s are confined in the observing plane P_{observ}. Actually, the *SVZ*s and *CFZ*s also occupy some zone space along the *z*-direction around the P_{observ}, as shown in Fig. 11. Here, only three lenses are drawn for simplicity. When the pupil deviates away from the P_{observ} along the negative *z*-direction, the *SVZ*s get enlarged while the *CFZ*s shrink. As a result, the changing rates of the observed transitional stereo-image will be sometimes faster and sometimes slower. This phenomenon can be seen more clearly in the online multimedia (Media 1). Inversely, if the pupil deviates away from the P_{observ} along the positive *z*-direction, this uneven changing rate gets remediated by some extent, but crosstalk noises from adjacent stereo-images will appear when the pupil is just centered at the viewpoints, i.e. the center points of each *SVZ*.

Once the pupil leaves away the plane determined by the points M'_{k-1}, M'_k, M'_{k+1}, a new kind of *CFZs* gets generated. $CFZ_{k-1\sim k\sim k+1}$ in the Fig. 12 is shown as an example. For an observation point in the $CFZ_{k-1\sim k\sim k+1}$, the observed transitional stereo-image is constituted by three segments from adjacent stereo-image *k-1*, *k* and *k + 1*, respectively. Although the presented transitional stereo-image still changes in a timed continuous manner under this condition, the difference between segments from the stereo-images *k-1* and *k + 1* becomes even more obvious, resulting in deterioration of the accuracy of the displayed *3D* image. Therefore, in order to display the *3D* image more accurately, the region between P_{observ} and the plane determined by the points M'_{k-1}, M'_k, M'_{k+1} is taken as the preferred observing zone along the *z*-direction, which is about 20.3*mm* in our prototype system.

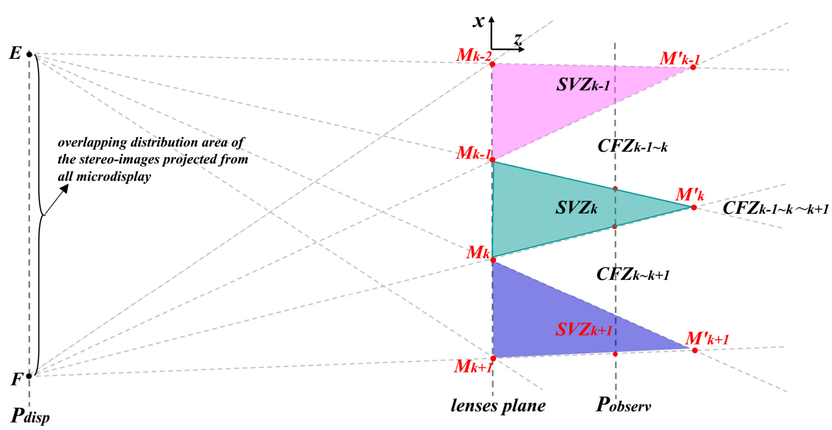

Fig. 12. Schematic diagram showing the spatial expansion of the *SVZ*s and *CFZ*s along the *z*-direction.

#232272 - $15.00 USD Received 12 Jan 2015; revised 15 Feb 2015; accepted 19 Feb 2015; published 25 Feb 2015

Another problem that needs to be addressed is the wavefront aberrations from the processed lenses, especially when the lenses have larger offsets with respect to their corresponding microdisplays. Experimentally, anti-distortion through a correction Table [19] is performed to alleviate the wavefront aberration for the lenses with larger offsets. The procedure of the anti-distortion correction can be illustrated by Fig. 13. A dot pattern, as shown in Fig. 13(a), functions as the target image and is loaded onto one microdisplay with all other microdisplays being shut down at the same time. The projected virtual image, as shown in Fig. 13(b), is captured at the corresponding *SVZ*. Through analyzing the distortion of the captured image, a correction table is generated. An anti-distorted image is obtained based on the correction table, as shown in Fig. 13(c). Loading the anti-distorted image onto this microdisplay, a corrected image gets displayed, as shown in Fig. 13(d). This process is performed for each microdisplay-lens pairs and all stereo-images are anti-distorted through establishing their respective correction tables.

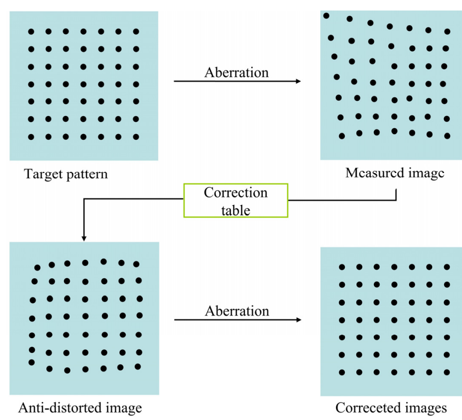

Fig. 13. Correction of the image distortion by the electronic method.

5. Conclusions

In conclusion, a novel multiview *3D* display with continuous motion parallax and full display resolution are realized through controllable spatial-spectrum fusing of light-rays from planar aligned *OLED* microdisplays. The proposed system needs only a thin optical structure (65*mm*) offering great potential for portable or mobile *3D* display applications provided that the related driving and control systems can be integrated into a monolithic chip. Compared with existing technologies to bypass the discontinuous motion parallax issue in multiview *3D* display, i.e. super-multiview display technique and viewer-tracking technique, the novel technology proposed in this paper can get implemented with a moderate number of *2D* display panels without using viewer-tracking unit. This endows our system with higher practicability.

Limited by *N.A* = 0.75 of the used lenses and the mechanical size of the *OLED* microdisplay, 9 *OLED* microdisplays are used by the prototype system in this manuscript and a viewing angle of 13° is reached experimentally. If *OLED* microdisplays with a smaller size d_x are available and lenses with a larger *N.A.* are used, more natural motion parallax and wider viewing angles can be obtained through the proposed system. This is the focus of our future work.

Acknowledgments

The authors gratefully acknowledge support by the Natural Science Foundation of China, Grant No. U1201254, the National High Technology Research and Development Program of China (No. 2013AA03A106, No. 2015AA03A101).